Differential GPS aided Inertial Navigation: a Contemplative Realtime Approach

Sheng Zhao * **Yiming Chen** * **Haiyu Zhang** * **Jay A. Farrell** *

* *Dept. of Electrical Eng., U. of California, Riverside, 92521, USA*
(e-mail: szhao, yichen, hzhang, farrell@ee.ucr.edu)

Abstract: Extended Kalman Filtering (EKF) based GPS-INS has poor performance when there are strong nonlinearities. This limitation stems from the linearized nature of the EKF. This paper proposes a Contemplative Realtime (CRT) framework for Differential GPS aided inertial navigation. This method guarantees low latency for real-time application and meanwhile enhances the accuracy and reliability of navigation, especially in challenging urban environments. To realize these improvements, a Bayesian optimization based smoothing is combined with conventional filtering in an efficient way. For demonstration purpose, this CRT framework is implemented on an automotive vehicle with differential pseudorange and IMU measurements. The implementation result shows that compared to standard EKF method, the proposed approach could provide accurate vehicle navigation with robustness.

Keywords: Global Positioning System, Inertial Navigation, State Estimation, Kalman Filter

1. INTRODUCTION

Global Positioning System aided Inertial Navigation System (GPS-INS) is widely applied for navigation purpose on aircrafts, land vehicles, marine surface vehicles and other platforms (see Diesel (1991); Farrell et al. (2000); Bevly et al. (2006); Elkaim et al. (2008)). Due to the complimentary sensor properties, this GPS-INS integration has proven its efficiency under the framework of standard Extended Kalman Filter (EKF) (see Farrell (2008)). Especially, when carrier phase measurements and differential sources are available, the centimeter level accuracy can be achieved by applying Real Time Kinematic (RTK) technique (see Farrell et al. (2000)). However, conventional GPS-INS still has limitations, among which is that the performance of the EKF significantly depends on initial conditions and nonlinearities (see Dellaert and Kaess (2006)). This is due to the fact that previous improper EKF linearization points cannot be corrected at later times.

To overcome this inconsistence problem of the EKF method, a smoothing approach has attracted considerable attention in the Simultaneous Localization and Mapping (SLAM) research community (see Dellaert and Kaess (2006); Kaess et al. (2008, 2012)). A key point of smoothing in the SLAM context is keeping the complete robot trajectory in the estimation, so all the useful information over the time window can be considered to reach statistically optimality. By exploring the sparsity of the involved matrices and introducing incremental solution, the smoothing approach is claimed to be fast and efficient (see Kaess et al. (2008)). However, for real-time inertial vehicle navigation and control applications, where temporal latency can cause severe issues, the computational cost is still fairly considerable.

In this paper, a novel GPS-INS framework is proposed for accurate and reliable vehicle navigation. The proposed approach, which is referred as a Contemplative Realtime (CRT) method, guarantees not only real-time performance, but also precision and robustness, by combining filtering, smoothing and outlier rejection in an efficient way. In the smoothing, a *Maximum-a-Posteriori* (MAP) optimization is formed by considering all the information over an extended duration window. Statistical testing procedures are introduced to detect, identify and remove erroneous GPS measurements during the smoothing process. The measurement redundancy in the outlier detection is improved, since a whole window of measurements are included. For demonstration, this CRT GPS-INS is implemented with differential compensated pseudorange and IMU measurements on an automotive vehicle. The implementation result shows that the proposed framework enhances navigation accuracy and reliability.

The overall GPS-INS positioning accuracy will be determined by the GPS performance. However, faulty GPS measurements can be caused by many factors. For example, drastic atmospheric variations or multipath effects could delay the signal. Receiver Autonomous Integrity Monitoring (RAIM, see Hewitson et al. (2004); Bhatti (2007)) is a set of techniques to check the consistency of measurements relying on measurement redundancy. Conventional RAIM only uses measurements from one epoch, which cannot always guarantee enough available satellites. One way to fix this RAIM 'hole' is to integrate external aiding like INS. Several papers have considered such extended RAIM (eRAIM, see Hewitson and Wang (2010)) using linearized propagation methods over two measurement times. The methods herein extend these ideas over $K > 1$ epochs while addressing the full nonlinear solution.

This paper is organized as follows. Section 2 presents the problem statement. Section 3 introduces the CRT approach. Section 4 presents the details of the *Maximum-a-Posteriori* problem. Section 5 gives a brief discussion

of reliable removal of faulty data in the CRT framework. Section 6 shows the experimental results with vehicle data.

2. PROBLEM STATEMENT

This section introduces the background and notation of differential GPS aided inertial navigation. The main INS and GPS references for this presentation are Farrell (2008) and Misra and Enge (2001), respectively, which should be consulted for additional information.

2.1 Aided Inertial Navigation

Let $\boldsymbol{x} \in \mathbb{R}^n$ denote the rover state vector. The kinematic equations for the rover state are

$$\dot{\boldsymbol{x}}(t) = \boldsymbol{f}(\boldsymbol{x}(t), \boldsymbol{u}(t)), \tag{1}$$

where $\boldsymbol{f} : \mathbb{R}^n \times \mathbb{R}^m \mapsto \mathbb{R}^n$ and $\boldsymbol{u} \in \mathbb{R}^m$ is the vector of accelerations and angular rates. The function $\boldsymbol{f}$ is accurately known (see Chapter 11 in Farrell (2008)).

Given a distribution for the state vector initial condition $\boldsymbol{x}(0) \sim N(\hat{\boldsymbol{x}}(0), \boldsymbol{P}(0))$ and measurements $\tilde{\boldsymbol{u}}$ of $\boldsymbol{u}$, an Inertial Navigation System (INS) propagates an estimate of the vehicle state between aiding measurement times as a solution of

$$\dot{\hat{\boldsymbol{x}}}(t) = \boldsymbol{f}(\hat{\boldsymbol{x}}(t), \tilde{\boldsymbol{u}}(t)), \tag{2}$$

where $\hat{\boldsymbol{x}}(t)$ denotes the estimate of $\boldsymbol{x}(t)$.

Due to initial condition errors, system calibration errors, and measurement noise, the state estimation error $\delta\boldsymbol{x}(t) = \boldsymbol{x}(t) - \hat{\boldsymbol{x}}(t)$ develops over time. The dynamics and stochastic properties of this estimation error are well understood.

When aiding measurements

$$\tilde{\boldsymbol{z}}(t) = \boldsymbol{h}(\boldsymbol{x}(t)) + \boldsymbol{n}_z(t) \tag{3}$$

are available, various methods are available to use the initial state, inertial measurements, and aiding measurement information to estimate the vehicle state vector (Farrell (2008); Kay (1993)).

2.2 DGPS Pseudorange Measurements

Throughout this article, double differenced GPS measurements are considered. For simplicity of notation, it is assumed that DGPS approach completely removes all common-mode errors (e.g., ionosphere, troposphere, satellite clock and ephemeris errors). The code (pseudorange) measurements for the $i-$th satellite can be modeled as

$$\bar{\boldsymbol{\rho}}^i = \bar{R}^i + c\boldsymbol{\delta}t_r + \bar{\boldsymbol{n}}^i_\rho, \tag{4}$$

where $\bar{R}^i(t) = \|\boldsymbol{p}(t) - \boldsymbol{p}^i(t)\|_2$ is the geometric distance between the vehicle position $\boldsymbol{p} \in \mathbb{R}^3$ and $\boldsymbol{p}^i \in \mathbb{R}^3$ is the $i-$th satellite position, $c\boldsymbol{\delta}t_r \in \mathbb{R}$ is the receiver clock bias, $\bar{\boldsymbol{n}}^i_\rho$ is the measurement noise. Subtracting all satellite's measurements by a common satellite's measurement will remove the clock bias $c\boldsymbol{\delta}t_r$. The new measurement model after double difference is:

$$\boldsymbol{\rho}^i = R^i + \boldsymbol{n}^i_\rho, \tag{5}$$

where $R^i(t) = \bar{R}^i(t) - \bar{R}^{com}(t)$, $\boldsymbol{\rho}^i = \bar{\boldsymbol{\rho}}^i - \bar{\boldsymbol{\rho}}^{com}$ and $\boldsymbol{n}^i_\rho = \bar{\boldsymbol{n}}^i_\rho - \bar{\boldsymbol{n}}^{com}_\rho$.

Thus, the code measurement in eqn. (5) conforms with the standard measurement model represented in eqn. (3).

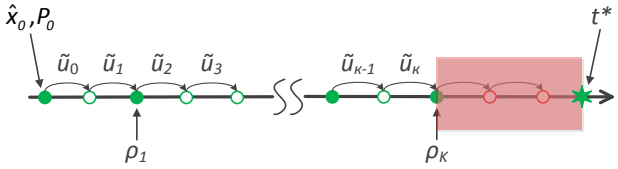

Fig. 1. Measurement timeline for one CRT cycle.

2.3 Technical Problem Statement

This paper considers vehicle state estimation problem using inertial and DGPS pseudorange measurements. Without loss of generality, we consider the problem on the time interval $[t_0, t_K]$, which contains K GPS measurement time instants, where K can be designer specified, time varying, or data dependent. The technical problem can be stated as follows.

For a system described by eqn. (1), we have

- an initial distribution for the state $\boldsymbol{x}(t_0)$,
- IMU measurements $\mathbf{U} = \{\tilde{\boldsymbol{u}}(\tau_k)\}_{k=0}^{\kappa}$,
- DGPS code measurements $\mathbf{Y} = \{\mathbf{Y}(t_j)\}_{j=1}^{K}$, where $\mathbf{Y}(t_j) = \{\boldsymbol{\rho}^i(t_j)\}_{i=1}^{m_j}$.

where $t_0,\ t_j \in (\tau_0, \tau_\kappa]$ and $m_j = m(t_j)$ is the total number of available satellites at t_j. For convenience of notation later, let $\{t_k\}_{k=0}^{K} = \{t_0\} \cup \{t_j\}_{j=1}^{K} \subset [t_0, t_K]$, such that the set of times is ordered and non-repeating. This interval of time will be referred to as the *CRT window*.

Then, we have the *objective*: Estimate the optimal state trajectory $\mathbf{X} = \{\boldsymbol{x}(t_k)\}_{k=0}^{K}$ with the given sensor measurements $\mathbf{U}$, $\mathbf{Y}$ and the prior state density $p_{\boldsymbol{x}}(\boldsymbol{x}(t_0))$.

3. CONTEMPLATIVE REALTIME APPROACH

This paper develops a Contemplative RealTime (CRT) approach proposed in Ramanandan et al. (2011); Chen et al. (2013) for the GPS INS data scenario described in Section 2.3. The CRT approach has both real-time and contemplative aspects. The real-time state estimate is required for control and planning purposes, without latency. The contemplative aspects are intended to enhance accuracy and reliability and are inspired by recent research in the field robotics literature, see e.g.: Dellaert and Kaess (2006); Kaess et al. (2008); Mourikis and Roumeliotis (2007); Li and Mourikis (2013).

A typical measurement scenario over the CRT window is depicted in Fig. 1. The contemplative process starts when $t = t_K$. At t_K, all IMU, GPS, and other measurements are available for the time interval $[t_0, t_K]$. A prior trajectory $\hat{\boldsymbol{x}}(\lambda)$ for $\lambda \in [t_0, t_K]$ is also available. Starting from this prior trajectory, the CRT algorithm will contemplate the available information to reliably and accurately compute the state trajectory over the CRT window using optimization shown in Dellaert and Kaess (2006); Kuemmerle et al. (2011) and statistical hypothesis testing methods discussed in Baarda (1968); Hewitson et al. (2004). This contemplative process ends at a time $t^* > t_K$, ideally providing an optimal trajectory estimate $\hat{\boldsymbol{x}}(\lambda)$ for $\lambda \in [t_0, t_K]$ from which the effects of sensor faults

have been removed. For the computation time interval $t \in [t_K, t^*]$, the real-time estimate of the realtime state estimate $\hat{\boldsymbol{x}}(t)$ is maintained by the INS using the IMU data and starting from the prior estimate of $\boldsymbol{x}(t_K)$. At $t = t^*$, $\hat{\boldsymbol{x}}(t_M)$ is corrected to the result of the CRT contemplative process and propagated through time using the IMU data and eqn. (2) to provide an improved estimate of $\boldsymbol{x}(t)$ at the present time. At some time $t \geq t^*$, the CRT window can be redefined and the process can repeat indefinitely.

Fig. 1 depicts a typical CRT window. The dots on the time-line indicate IMU measurement times τ_k. The state transition between these times is constrained by the kinematic model of eqn. (2) and the IMU data $\mathbf{U}$. Additional constraints are imposed by the initial state estimate, and GPS measurements $\mathbf{Y}$. The initial condition $(\hat{\boldsymbol{x}}(t_0), \boldsymbol{P}(t_0))$ constraints are shown above the time-line. The GPS measurement constraints ($\boldsymbol{\rho}$) are depicted below the time-line. Each of these constraints is quantified by a probability density that enables a Bayesian problem formulation. While Fig. 1 depicts all GPS measurements occurring at the IMU measurement time, unaligned measurements can be addressed by interpolation, and unknown latencies can be calibrated by the methods in Li and Mourikis (2014, to appear).

The main contribution of this article is the derivation and implementation of this Bayesian approach, particularly for the DGPS/INS application.

4. MAP ESTIMATION

Given the sensor measurements $\mathbf{U}$, $\mathbf{Y}$ and the prior state density $p_{\boldsymbol{x}}(\boldsymbol{x}(t_0))$, our objective is to compute the state trajectory $\mathbf{X} = \{\boldsymbol{x}(t_k)\}_{k=0}^{K}$ that maximizes the joint probability density $p(\mathbf{X}, \mathbf{Y}, \mathbf{U})$. Due to the use of the prior density at t_0, this is a *Maximum-A-Posteriori* (MAP) estimation problem.

The algorithm below builds upon the methods and notation standard for INS implementations, see e.g., Farrell (2008). For convenience, a very brief review of the method and notation are presented in the appendix .

4.1 Theoretical Solution

Using standard methods (see Chapters 10-11 in Kay (1993)) and assuming that $\boldsymbol{x}(t_0)$, $\boldsymbol{\omega}_u$ and $\boldsymbol{n}_\rho$ are all independent, the MAP estimate of $\mathbf{X}$ is

$$\hat{\mathbf{X}} = \arg\max_{\mathbf{X}} \Big(p_{\delta \boldsymbol{x}_0}\big(\boldsymbol{x}(t_0) - \boldsymbol{x}_0\big) \; p_{\boldsymbol{\omega}_u}\big(\mathbf{X}_+ - \boldsymbol{\phi}(\mathbf{X}, \mathbf{U})\big) p_{\boldsymbol{n}_\rho}\big(\mathbf{Y} - \boldsymbol{h}(\mathbf{X})\big)\Big), \tag{6}$$

where $\mathbf{X}_+ = \{\boldsymbol{x}(t) \text{ for } t = t_1, \ldots, t_K\}$, $\delta \boldsymbol{x}_0 = \big(\boldsymbol{x}(t_0) - \boldsymbol{x}_0\big) \sim \mathcal{N}(\mathbf{0}, \mathbf{P_0})$ and the operator $\boldsymbol{\phi}$ is defined in eqn. (18) in the appendix.

Direct maximization of eqn. (6) is complicated by various factors. First, each $\boldsymbol{x}(t_k) \in \mathbb{R}^n$ where in most applications $n \geq 15$. Second, both the kinematic model $\boldsymbol{f}$ and the measurement model $\boldsymbol{h}$ are nonlinear.

4.2 Solution Overview

The algorithm will involve two steps.

(1) Given an estimate of the solution

$$\hat{\mathbf{X}}^l = \left\{ \hat{\boldsymbol{x}}^l(t) \text{ for } t = t_0, \ldots, t_K \right\},$$

which is treated as a vector in $\mathbb{R}^{n(K+1)}$, an optimization algorithm computes a $\delta \boldsymbol{x}^l \in \mathbb{R}^{n(K+1)}$ such that

$$\hat{\mathbf{X}}^{l+1} = \hat{\mathbf{X}}^l + \delta \boldsymbol{x}^l \tag{7}$$

is an improved solution to eqn. (6). The optimization problem is formulated and solved in Section 4.4.

(2) Evaluation of the factor $p_{\boldsymbol{\omega}_u}\big(\mathbf{X}_+ - \boldsymbol{\phi}(\mathbf{X}, \mathbf{U})\big)$ of the MAP cost function and its linearization requires reintegration relative to $\hat{\mathbf{X}}^{l+1}$. This issue is subtle and will be clarified in Subsection 4.3.

4.3 Solution Detail: Reintegration

In this subsection, the subscript k is used to represent the time t_k for simplicity of notation. For example, $\hat{\boldsymbol{x}}_k^l = \hat{\boldsymbol{x}}^l(t_k), t_k = t_0, \ldots, t_K$.

Given $\hat{\mathbf{X}}^l$, the kinematic model provides an operator

$$\bar{\boldsymbol{x}}_{k+1}^l = \hat{\boldsymbol{x}}_k^l + \int_{t_k}^{t_{k+1}} f(\bar{\boldsymbol{x}}^l(\tau), \hat{\boldsymbol{u}}(\tau)) d\tau \tag{8}$$

with $\bar{\boldsymbol{x}}^l(t_k) = \hat{\boldsymbol{x}}_k^l$. Note that the quantity $\bar{\boldsymbol{x}}_{k+1}^l - \hat{\boldsymbol{x}}_{k+1}^l$ is not necessarily zero. The sequence $\hat{\boldsymbol{x}}_k^l$ results from optimization of eqn. (6), which involves a tradeoff between three factors, only one of which enforces the smooth trajectory constraint defined in eqn. (2). Therefore, even if $\hat{\mathbf{X}}^l$ satisfies eqn. (2), there is no guarantee, and in fact it is unlikely that $\hat{\mathbf{X}}^{l+1}$ resulting from eqn. (7) will exactly satisfy eqn. (2).

Similarly, the actual trajectory is generated according to

$$\boldsymbol{x}_{k+1} = \boldsymbol{x}_k + \int_{t_k}^{t_{k+1}} f(\boldsymbol{x}(\tau), \boldsymbol{u}(\tau)) d\tau. \tag{9}$$

For optimization, we will work with a linearization around $\{\hat{\boldsymbol{x}}_k^l\}_{k=0}^K$. The model for the time propagation of the error is:

$$\begin{aligned}
\boldsymbol{x}_{k+1} - \bar{\boldsymbol{x}}_{k+1}^l &= \boldsymbol{x}_k + \int_{t_k}^{t_{k+1}} f\big(\boldsymbol{x}(\tau), \boldsymbol{u}(\tau)\big) d\tau \\
&\quad - \hat{\boldsymbol{x}}_k^l - \int_{t_k}^{t_{k+1}} f\big(\bar{\boldsymbol{x}}^l(\tau), \hat{\boldsymbol{u}}(\tau)\big) d\tau. \\
\hat{\boldsymbol{x}}_{k+1}^l - \bar{\boldsymbol{x}}_{k+1}^l &= \boldsymbol{\Phi}_k \delta \boldsymbol{x}_k^l + \big(\hat{\boldsymbol{x}}_{k+1}^l - \boldsymbol{x}_{k+1}\big) + \boldsymbol{\omega}_k \\
\hat{\boldsymbol{x}}_{k+1}^l - \bar{\boldsymbol{x}}_{k+1}^l &= \boldsymbol{\Phi}_k \delta \boldsymbol{x}_k^l - \mathbf{I} \delta \boldsymbol{x}_{k+1}^l + \boldsymbol{\omega}_k.
\end{aligned} \tag{10}$$

As discussed in the appendix, the integration process that computes eqn. (8) also computes $\boldsymbol{\Phi}_k$ and $cov(\boldsymbol{\omega}_k) = \mathbf{Q}_k$.

4.4 Solution Detail: Optimization

For the derivation, we make the reasonable and standard assumptions that $\boldsymbol{\omega}_u \sim \mathcal{N}(\mathbf{0}, \mathbf{Q})$ is the IMU measurement noise, $\boldsymbol{n}_\rho \sim \mathcal{N}(\mathbf{0}, \mathbf{R}_\rho)$ and $\boldsymbol{x}(t_0) \sim \mathcal{N}(\boldsymbol{x}_0, \mathbf{P}_0)$, then in particular, $\delta \boldsymbol{x}_0 \sim \mathcal{N}(\mathbf{0}, \mathbf{P}_0)$. With various modifications, the derivation goes through for other distributions.

With these Gaussian noise assumptions, maximization of eqn. (6) is equivalent to minimization of

$$\begin{aligned}\|\mathbf{v}\|^2_{\mathbf{W}} = &\|\boldsymbol{x}(t_0) - \boldsymbol{x}_0\|_{\mathbf{P}_0} \\ &+ \sum_k \|\boldsymbol{\phi}\big(\boldsymbol{x}(t_k), \mathbf{U}_k\big) - \boldsymbol{x}(t_{k+1})\|_{\mathbf{Q}_k} \\ &+ \sum_j \sum_i \|\boldsymbol{h}^i_j\big(\boldsymbol{x}(t_j)\big) - \boldsymbol{\rho}^i(t_j)\|_{{}^i_j\mathbf{R}_\rho} \end{aligned} \tag{11}$$

where $\|\mathbf{v}\|^2_{\mathbf{W}} = \mathbf{v}^\top \mathbf{W}^{-1}\mathbf{v}$ is the squared Mahalanobis distance with the matrix $\mathbf{W}$ and the operator $\boldsymbol{\phi}$ is defined in the appendix. The vector $\mathbf{v}$ is the concatenation of each of the vectors summed in the right-hand side of eqn. (11) and $\mathbf{W}$ is the postive definite block diagonal matrix formed by the positive definite submatrices ${}^i_j\mathbf{R}_\rho$, $\mathbf{P}_0$ and $\mathbf{Q}_k$.

Note that $\|\mathbf{v}\|_{\mathbf{W}} = \|\boldsymbol{r}\|_2$ where $\boldsymbol{r} \triangleq \boldsymbol{\Sigma}_W \mathbf{v}$ and $\mathbf{W}^{-1} = \boldsymbol{\Sigma}_W^\top \boldsymbol{\Sigma}_W$. In particular,

$$\boldsymbol{r}(\mathbf{X}) = \begin{bmatrix} \boldsymbol{\Sigma}_{\mathbf{P}_0}\big(\boldsymbol{x}(t_0) - \boldsymbol{x}_0\big) \\ \hline \boldsymbol{\Sigma}_{\mathbf{Q}_0}\big(\boldsymbol{\phi}\big(\boldsymbol{x}(t_0), \mathbf{U}_0\big) - \boldsymbol{x}(t_1)\big) \\ \vdots \\ \boldsymbol{\Sigma}_{\mathbf{Q}_{K-1}}\big(\boldsymbol{\phi}\big(\boldsymbol{x}(t_{K-1}), \mathbf{U}_{K-1}\big) - \boldsymbol{x}(t_K)\big) \\ \hline \boldsymbol{\Sigma}_{{}^1_1\mathbf{R}_\rho}\big(\boldsymbol{h}^1_1\big(\boldsymbol{x}(t_1)\big) - \boldsymbol{\rho}^1(t_1)\big) \\ \vdots \\ \boldsymbol{\Sigma}_{{}^{m_1}_1\mathbf{R}_\rho}\big(\boldsymbol{h}^{m_1}_1\big(\boldsymbol{x}(t_1)\big) - \boldsymbol{\rho}^{m_1}(t_1)\big) \\ \hline \vdots \\ \hline \boldsymbol{\Sigma}_{{}^1_K\mathbf{R}_\rho}\big(\boldsymbol{h}^1_K\big(\boldsymbol{x}(t_K)\big) - \boldsymbol{\rho}^1(t_K)\big) \\ \vdots \\ \boldsymbol{\Sigma}_{{}^{m_K}_K\mathbf{R}_\rho}\big(\boldsymbol{h}^{m_K}_K\big(\boldsymbol{x}(t_K)\big) - \boldsymbol{\rho}^{m_K}(t_K)\big) \end{bmatrix}. \tag{12}$$

With this notation, the minimization problem of eqn. (11) reduces to a nonlinear least square optimization

$$\min_{\mathbf{X}\in\mathbb{R}^{n(K+1)}} \|\boldsymbol{r}(\mathbf{X})\|^2_2. \tag{13}$$

Standard iterative methods (e.g. Gauss-Newton, gradient descent, Levenberg-Marquardt) are applicable.

The Gauss-Newton step $\boldsymbol{\delta}_{gn}$ can be derived by solving,

$$\mathbf{J}^\top \mathbf{J}\delta\boldsymbol{x} = -\mathbf{J}^\top \boldsymbol{b} \tag{14}$$

where

$$\boldsymbol{b} \triangleq \boldsymbol{r}(\hat{\mathbf{X}}) = \begin{bmatrix} \boldsymbol{\Sigma}_{\mathbf{P}_0}\big(\hat{\boldsymbol{x}}(t_0) - \boldsymbol{x}_0\big) \\ \hline \boldsymbol{\Sigma}_{\mathbf{Q}_0}\big(\bar{\boldsymbol{x}}_1 - \hat{\boldsymbol{x}}_1\big) \\ \vdots \\ \boldsymbol{\Sigma}_{\mathbf{Q}_{K-1}}\big(\bar{\boldsymbol{x}}_K - \hat{\boldsymbol{x}}_K\big) \\ \hline \boldsymbol{\Sigma}_{{}^1_1\mathbf{R}_\rho}\big(\boldsymbol{h}^1_1\big(\hat{\boldsymbol{x}}(t_1)\big) - \boldsymbol{\rho}^1(t_1)\big) \\ \vdots \\ \boldsymbol{\Sigma}_{{}^{m_1}_1\mathbf{R}_\rho}\big(\boldsymbol{h}^{m_1}_1\big(\hat{\boldsymbol{x}}(t_1)\big) - \boldsymbol{\rho}^{m_1}(t_1)\big) \\ \hline \vdots \\ \hline \boldsymbol{\Sigma}_{{}^1_K\mathbf{R}_\rho}\big(\boldsymbol{h}^1_K\big(\hat{\boldsymbol{x}}(t_K)\big) - \boldsymbol{\rho}^1(t_K)\big) \\ \vdots \\ \boldsymbol{\Sigma}_{{}^{m_K}_K\mathbf{R}_\rho}\big(\boldsymbol{h}^{m_M}_K\big(\hat{\boldsymbol{x}}(t_K)\big) - \boldsymbol{\rho}^{m_K}(t_K)\big) \end{bmatrix}$$

and $\mathbf{J}$ is the Jacobian matrix of $\boldsymbol{r}(\mathbf{X})$ evaluated at $\hat{\mathbf{X}}^l$. In the vector $\boldsymbol{b}$, the residuals $\bar{\boldsymbol{x}}_k - \hat{\boldsymbol{x}}_k$ are computed by the method in Subsection 4.3. The inverse covariance weighted Jacobian matrices in $\mathbf{J}$ can be demonstrated well-defined.

When solving for $\delta\boldsymbol{x}$ in eqn. (7), to save the computation as shown in Kuemmerle et al. (2011), we form the equation: $\boldsymbol{\Lambda}\delta\boldsymbol{x} = \boldsymbol{\eta}$, where $\boldsymbol{\Lambda} = \mathbf{J}^\top\mathbf{J}$, $\boldsymbol{\eta} = -\mathbf{J}^\top\boldsymbol{b}$. This equation can be solved efficiently by the Cholesky factorization as discussed in Dellaert and Kaess (2006).

4.5 Marginalization

Due to the computational resource constraints, we cannot save the entire past history of states in the CRT window. The Schur complement is employed to marginalize out the oldest states from the CRT window and generate a new prior state density, see Dong-Si and Mourikis (2011).

5. RELIABLE REMOVAL OF FAULTY DATA

Receiver Autonomous Integrity Monitoring (RAIM, Hewitson et al. (2004)) is a set of techniques to detect, identify and remove GNSS receiver outlier measurements. Traditionally, in the navigation community, RAIM is designed assuming only one outlier occurs and that there is enough measurement redundancy to detect and identify the source. The proposed CRT approach, which enhances the redundancy by incorporating a window of IMU and GPS data, can be expected to enable multiple outlier detection, identification, and removal. This outlier rejection scheme, which enhances the robustness of vehicle GPS-INS significantly, could make critical contributions as necessary for life-safety applications. The key technique in standard RAIM is *outlier detection and identification*. This section considers the detection and identification, removal procedures within the CRT framework. Interested readers may find more details in Hewitson et al. (2004).

Suppose that the MAP optimization in eqn. (13) finally converges to a optimal estimate $\mathbf{X}^*$. The generalized *a-posteriori* variance factor test evaluated as

$$\hat{\sigma}^2_0 = \frac{\|\boldsymbol{r}(\mathbf{X}^*)\|^2_2}{M - N}, \tag{15}$$

can be used to detect outlier. In this expression, $M = n(1+K) + \sum_{j=1}^K (m_j - 1)$ is the total number of residuals (constraints) and $N = n(K+1)$ is the dimension of $\mathbf{X}$. Note that $\sum_{j=1}^K (m_j - 1)$ is the total number of double-differenced GPS measurements. The degrees-of-freedom $(M - N)$ can be considered as the index of the measurement redundancy. For conventional GNSS-only RAIM which uses one epoch measurements, the redundancy is $(m_j - 4)$, which requires at least five satellites to be available. For the proposed CRT framework, the measurement redundancy is $M - N = \sum_{j=1}^K (m_j - 1)$, which indicates that it has enhanced detectability against faulty data.

The final step of outlier detection is to test the above variance factor against the two-tailed Chi-square test limits with respect to a significance level α,

$$\frac{\chi^2_{1-\alpha/2, M-N}}{M-N} \leq \hat{\sigma}^2_0 \leq \frac{\chi^2_{\alpha/2, M-N}}{M-N}. \tag{16}$$

If the test succeeds, $\mathbf{X}^*$ is finalized as the smoothing result and the real-time part will use it to reinitialize. If not, outlier identification executes by testing each residual with the w-test. Once the source of the outlier is identified, the corresponding measurement will be removed and the procedure continues until no additional outliers are identified.

Fig. 2. Vehicle trajectory (red). The yellow and blue markers show the start and end points, respectively.

When outlier identification completes, the outliers are removed and the MAP optimization is formed with the cleaned-up measurement set, then the detect-identify-remove procedure repeats.

6. EXPERIMENTAL RESULTS

This section uses 200Hz MEMS IMU and 1Hz Differential GPS data collected on a vehicle. The estimator is implemented in C++ and runs at 200 Hz in realtime to report the realtime vehicle state estimate. In this experiment, the vehicle stays stationary while pointing north at the beginning. After about 20 seconds the vehicle accelerated north. The trajectory of vehicle is illustrated in Fig. 2.

This section compares the following real-time estimators:

(1) CRT using double-differenced code measurements;
(2) EKF using double-differenced code measurements;
(3) EKF using integer-resolved double-differenced carrier phase measurements.

The definition of the state vector is the same for all cases. In addition, we post-process the data through an off-line batch smoother for the entire trajectory using integer-resolved double-differenced carrier phase and code measurements. This post-processed trajectory will be considered as the ground truth to which the other three estimators are compared to determine error statistics.

Firstly, we demonstrate the capability of the proposed estimator to initialize yaw, without a compass. For a stationary vehicle, yaw is unobservable from GPS measurements. When the vehicle accelerates, yaw becomes observable. For the EKF, the yaw needs to be initialized close to the true value to satisfy the EKF small error assumption; otherwise the EKF may diverge. For EKF implementations, yaw may be initialized via magnetometer, or other means. The CRT estimator optimally initialize the yaw using the data in the CRT window. Everything is done naturally within the smoothing framework and it is also optimal with respect to the pre-defined noise model. To demonstrate this, the initial yaw is set to have an error of 180 degrees. Fig. 3 shows that, when the vehicle accelerates (near $t = 20s$), the yaw rapidly converges toward the correct value.

Secondly, the proposed estimator significantly improves the state estimate accuracy. Fig. 4, Fig. 5 and Table 1 compare the estimated trajectory error from the three estimators mentioned above. Fig. 4 shows a segment of the estimated trajectories. The trajectory of the CRT

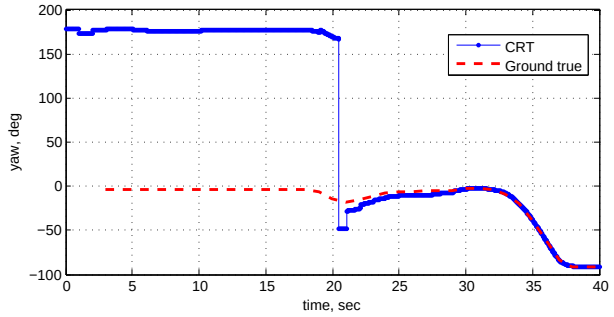

Fig. 3. Yaw estimated of the CRT estimator.

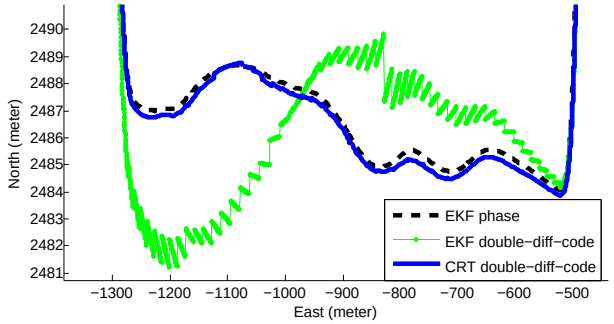

Fig. 4. EKF and CRT Position accuracy comparison.

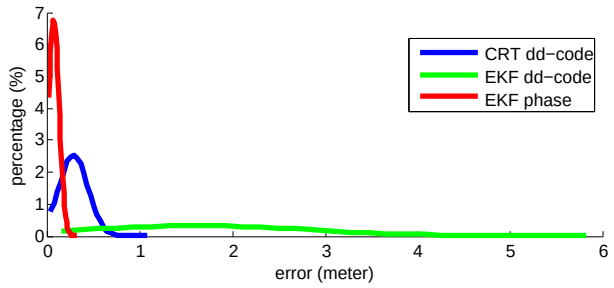

Fig. 5. Distribution of horizontal position error.

approach using double-differenced code is very near the trajectory of the EKF using double-differenced integer-resolved phase. The EKF using double-differenced code has significantly larger errors. The statistic comparison of the position error in the north and east directions over the entire trajectory is given in Table. 1. The distribution of the norm of the position error in the horizontal plane (north-east) is shown in Fig. 5. The statistics shown in Table 1 and Fig. 5 use the state estimate data at 1 Hz (324 data points in total for this trajectory). The error statistics clearly show that the proposed estimator has the position estimate error in the decimeter level, while the EKF using the same code measurements has the error in the meter level. This large accuracy improvement is gain by leveraging a window of measurements. The performance of the proposed estimator is already very close to that of the EKF using phase measurement (centimeter level). However, to achieve the centimeter accuracy, the integer ambiguity needs to be resolved in realtime.

7. DISCUSSION AND FUTURE WORK

This paper has presented a novel GPS-INS framework which is referred as a CRT estimator. Using the proposed framework, we demonstrated that yaw initialization can be

Table 1. Comparison of position error statistics

	North	East
CRT (dd-code):	$\mu = -0.016,\ \sigma = 0.18$	$\mu = 0.164,\ \sigma = 0.21$
EKF (dd-code):	$\mu = 0.162,\ \sigma = 1.69$	$\mu = 0.326,\ \sigma = 1.08$
EKF (phase):	$\mu = 0.001,\ \sigma = 0.05$	$\mu = -0.015,\ \sigma = 0.06$

done naturally and correctly without a magnetometer or ad-hoc methods as may be required for EKF approaches. In addition, the state estimate accuracy is enhanced significantly with respect to an EKF that uses exactly the same measurements. In addition, we envision that the proposed framework has the potential to allowing enhanced outlier rejection to ensure the robustness of the estimator. Interesting future work directions include development, implementation, and test of the outlier rejection approach, and incorporation of carrier phase and doppler measurements.

ACKNOWLEDGEMENTS

This research builds on the software of and technical conversations with Anastasios I. Mourikis and Mingyang Li. These technical collaborations are greatly appreciated.

REFERENCES

Baarda, W. (1968). A Testing Procedure for Use in Geodetic Networks. *Netherlands Geod. Comm.*, 2(4).

Bevly, D., Ryu, J., and Gerdes, J. (2006). Integrating INS Sensors with GPS Measurements for Continuous Estimation of Vehicle Sideslip, Roll, and Tire Cornering Stiffness. *IEEE Trans. ITS,*, 7(4), 483–493.

Bhatti, U. (2007). *Improved integrity algorithms for integrated GPS/INS systems in the presence of slowly growing errors.* Ph.D. thesis, Imperial College London.

Chen, Y., Zheng, D., Miller, P.M., and Farrell, J. (2013). Underwater Vehicle Near Real Time State Estimation. In *Proc. IEEE MSC.*

Dellaert, F. and Kaess, M. (2006). Square Root SAM: Simultaneous Localization and Mapping via Square Root Information Smoothing. *Int. J. Rob. Res.*, 25(12), 1181–1203.

Diesel, J. (1991). GPS/INS Integration for Civil Aviation. In *Proc. NTC*, 223–228.

Dong-Si, T.C. and Mourikis, A.I. (2011). Motion tracking with fixed-lag smoothing: Algorithm and consistency analysis. In *IEEE ICRA*, 5655–5662.

Elkaim, G., Lizarraga, M., and Pedersen, L. (2008). Comparison of low-cost GPS/INS sensors for Autonomous Vehicle applications. In *IEEE/ION PLANS*, 1133–1144.

Farrell, J., Givargis, T., and Barth, M. (2000). Real-time Differential Carrier Phase GPS-aided INS. *IEEE Trans. CST*, 8(4), 709–721.

Farrell, J.A. (2008). *Aided Navigation: GPS with High Rate Sensors.* McGraw Hill.

Hewitson, S. and Wang, J. (2010). Extended Receiver Autonomous Integrity Monitoring (eRAIM) for GNSS/INS Integration. *Journal of Surveying Eng.*, 136(1), 13–22.

Hewitson, S., Lee, H.K., and Wang, J. (2004). Localizability Analysis for GPS/Galileo Receiver Autonomous Integrity Monitoring. *J. of Navigation*, 57, 245–259.

Kaess, M., Johannsson, H., Roberts, R., Ila, V., Leonard, J., and Dellaert, F. (2012). iSAM2: Incremental smoothing and mapping using the Bayes tree. *Intl. J. of Robotics Research*, 31(2), 216–235.

Kaess, M., Ranganathan, A., and Dellaert, F. (2008). iSAM: Incremental Smoothing and Mapping. *IEEE Trans. Robotics,*, 24(6), 1365–1378.

Kay, S.M. (1993). *Fundamentals of Statistical Signal Processing, Estimation theory.* Prentice Hall PTR.

Kuemmerle, R., Grisetti, G., Strasdat, H., Konolige, K., and Burgard, W. (2011). g2o: A general framework for graph optimization. In *Proc. ICRA.*

Li, M. and Mourikis, A.I. (2013). High-Precision, Consistent EKF-based Visual-Inertial Odometry. *International J. of Robotics Research*, 32(6).

Li, M. and Mourikis, A.I. (2014, to appear). Online Temporal Calibration for Camera-IMU Systems: Theory and Algorithms. *International J. of Robotics Research.*

Misra, P. and Enge, P. (2001). *GPS: Signals, Measurements, and Performance.* Ganga-Jamma Press.

Mourikis, A. and Roumeliotis, S. (2007). A Multi-State Constraint Kalman Filter for Vision-aided Inertial Navigation. In *IEEE ICRA*, 3565–3572.

Ramanandan, A., Chen, A., and Farrell, J. (2011). A Near-Real Time Nonlinear State Estimation Approach with Application to Initialization of Navigation Systems. In *Proc. 50th IEEE CDC.*

APPENDIX I: INS REVIEW

For any initial state $\boldsymbol{x}(\tau_k)$, the solution to (1) for $t \in [\tau_k, \tau_{k+1}]$ is

$$\boldsymbol{x}(t) = \boldsymbol{x}(\tau_k) + \int_{\tau_k}^{t} \mathbf{f}(\mathbf{x}(\tau), \mathbf{u}(\tau))\mathbf{d}\tau. \tag{17}$$

While nature solves (17) in continuous time, the INS only has IMU and aiding measurements at discrete time instants; therefore, the INS numerically solves

$$\begin{aligned}\hat{\boldsymbol{x}}(\tau_{k+1}) &= \boldsymbol{\phi}\big(\hat{\boldsymbol{x}}(\tau_k), \hat{\boldsymbol{u}}(\tau_k)\big) \\ &= \hat{\boldsymbol{x}}(\tau_k) + \int_{\tau_k}^{\tau_{k+1}} \mathbf{f}(\hat{\mathbf{x}}(\tau), \hat{\mathbf{u}}(\tau))\mathbf{d}\tau. \end{aligned} \tag{18}$$

The result of the numeric integration of (18) is the INS state estimate of $\hat{\boldsymbol{x}}(\tau_{k+1})$ given $\hat{\boldsymbol{x}}(\tau)$ and $\hat{\boldsymbol{u}}(\tau)$. The numeric integration repeats to propagate the state measurements between the times of aiding measurements. The aiding measurement times can be unequally spaced in time without causing any complications.

Let $\hat{\mathbf{U}}_j = \{\hat{\boldsymbol{u}}(\tau_k),\ \tau_k \in [t_j, t_{j+1}]\}$, then eqn. (18) can be called recursively to compute $\hat{\boldsymbol{x}}(t_{j+1})$ from $\hat{\boldsymbol{x}}(t_j)$ and $\mathbf{U_j}$, denote this as

$$\hat{\boldsymbol{x}}(t_{j+1}) = \boldsymbol{\phi}\big(\hat{\boldsymbol{x}}(t_j), \hat{\mathbf{U}}_j\big). \tag{19}$$

At the same time, nature is integrating eqn. (17) which it denoted as

$$\boldsymbol{x}(t_{j+1}) = \boldsymbol{\phi}\big(\boldsymbol{x}(t_j), \mathbf{U}_j\big). \tag{20}$$

The linearized error growth model is

$$\delta\hat{\boldsymbol{x}}(t_{j+1}) = \boldsymbol{\Phi}_j \delta\hat{\boldsymbol{x}}(t_j) + \boldsymbol{\omega}_j \tag{21}$$

where $\boldsymbol{\omega}_j \sim N(0, \mathbf{Q}_j)$ and $\boldsymbol{\Phi}_j = \left.\frac{\partial \boldsymbol{\phi}(\boldsymbol{x})}{\partial \boldsymbol{x}}\right|_{(\hat{\boldsymbol{x}}(t_j), \hat{\mathbf{U}}_j)}$. The symbol $\boldsymbol{\omega}_u$ will be used to represent $\{\boldsymbol{\omega}_j\}_{j=1}^{K}$. The INS provides both $\mathbf{Q}_j$ and $\boldsymbol{\Phi}_j$, see Section 7.2.5.2 in Farrell (2008).